

DRAFT VERSION FEBRUARY 22, 2022

Typeset using L^AT_EX default style in AASTeX631

Spectral Lag Transition of 32 Fermi Gamma-ray Bursts and their Application on Constraining Lorentz Invariance Violation

ZI-KE LIU,^{1,2} BIN-BIN ZHANG,^{1,2} AND YAN-ZHI MENG^{1,2}

¹*School of Astronomy and Space Science, Nanjing University, Nanjing 210093, China*

²*Key Laboratory of Modern Astronomy and Astrophysics (Nanjing University), Ministry of Education, China*

ABSTRACT

The positive-to-negative transition of spectral lag is an uncommon feature reported in a small number of GRBs. An application of such a feature has been made to constrain the critical quantum gravity energy (E_{QG}) of the light photons under the hypothesis that the Lorentz invariance might be violated. Motivated by previous case studies, this paper systematically examined the up-to-date *Fermi*/GBM GRB sample for the lag transition feature to establish a comprehensive physical limit on the Lorentz Invariance Violation (LIV). This search resulted in 32 GRBs with redshift available, which exhibit the lag-transition phenomenon. We first fit each of the lag-E relations of the 32 GRBs with an empirical smoothly broken power law function, and found that the lag transition occurs typically at about 400 keV. We then implemented the LIV effect into the fit, which enabled us to constrain the lower limit of the linear and quadratic values of E_{QG} , which are typically distributed at 1.5×10^{14} GeV and 8×10^5 GeV, respectively.

1. INTRODUCTION

The spectral lag of Gamma-ray Bursts (GRBs) was first introduced by Norris et al. (1996) to describe the phenomenon that GRB light curves in higher energy bands peak earlier than those in lower energy bands. Subsequent studies (e.g., Norris et al. 2000; Yi et al. 2006) showed that long GRBs are always characterized by significant lags, whereas short GRBs always present zero, sometimes negative, lags. On the other hand, the exact physical mechanism that causes spectral lags remains incompletely resolved to date. Considering the relativistic beaming nature of a GRB jet, one may naturally expect that the so-called “high-latitude” effect can cause photons at higher latitudes to arrive at the observer later and with softened observed energy. Such effect was used by Salmonson (2000); Ioka & Nakamura (2001); Norris & Bonnell (2006) to explain the overall statistical properties of the observed lags as well as the luminosity-lag correlation (Schaefer 2004). By assuming an intrinsic spectral shape and a temporal profile, Shen et al. (2005) found that curvature effect marginally interpreted the observed lags, yet extreme physical parameter values are required. Furthermore, Uhm & Zhang (2016) demonstrated that the high-latitude curvature effect alone was not sufficient to account for the spectral lags. Rather, one must consider the intrinsic curved spectral shape, the evolution of the magnetic field strength, and the rapid bulk acceleration of the emission zone to interpret some observed spectral lag features. The aforementioned theories successfully explain the positive lags, however the rarely observed negative lags remain a more complex matter that can be used to infer the different radiation origins (Zhang et al. 2011), radiation mechanisms (Li 2010; Zhang et al. 2011), or emission regions (Toma et al. 2009) of low and high energy photons.

In the context the fundamental physics, the delay of high energy photons, formulated as negative lag in this study, can be used to test the violations of Lorentz invariance, a hypothesis that is widely pursued in quantum gravity (QG). LIV occurs at the Planck energy scale ($E_{\text{P1}} = \sqrt{\hbar c^5/G} \simeq 1.22 \times 10^{19}$ GeV) in QG theories (Mattingly 2005; Amelino-Camelia 2013). The LIV effect can be manifested through vacuum dispersion, which leads photons with higher energy

Corresponding author: Bin-Bin Zhang
bbzhang@nju.edu.cn

to travel at lower speeds (Amelino-Camelia et al. 1998). GRBs are one of the ideal probes for testing LIV due to their large cosmological distance, small variability time scale, and very high energy photons. Using the delay time of individual photons reaching a few GeV, several studies (e.g., Abdo et al. 2009a,b; Acciari et al. 2020) have shown that the linear QG energy scale, E_{QG} , can be constrained at $\gtrsim 10^{18-19}$ GeV. In order to further constrain the LIV effect, the most optimal use of lag to date has been to fit the keV-MeV multi-wavelength measurements of spectral lags, including their positive-to-negative transitions, with a model incorporating LIV information. A fit of this type yields some deeper limits on the QG energy (see e.g., Wei et al. 2017; Du et al. 2021). This approach has, however, only been applied in a few GRBs. A systematic study is required to determine whether the positive-to-negative transition is common in a large sample of GRBs and, if possible, to identify some additional constraints on the LIV effect according to the large sample lag data.

In this *Letter*, we utilize the *Fermi*/GBM GRB catalog to analyze all z-known GRBs with positive-to-negative lag transitions and use these results to place some further constraints on the LIV effect. Data selection and reduction are described in §2. Our model of the spectral lag is presented in §3. The constraints on LIV and fitting results with our model are presented in section §4, followed by a brief summary and discussion in §5.

2. DATA

To date, more than a thousand GRBs have been observed by *Fermi*/GBM (von Kienlin et al. 2020), of which 135 long-duration bursts with redshift are measured. These bursts constitute our initial sample which is further screened for the positive-to-negative lag transitions. The final sample for this study, as shown in Table 1, includes 32 GRBs. For each GRB, we extracted its multi-wavelength light curves and calculated its lags using the following steps.

1. Light curve extraction. In accordance with Yang et al. (2020); Zhang et al. (2021); Wang et al. (2021), we selected the time-tagged event (TTE) data from the Sodium Iodide (NaI) Scintillation and Bismuth Germanate (BGO) Scintillation detectors onboard Fermi/GBM that had the smallest separation from the location of the burst. Using those data, we then extract the multi-wavelength light curves in a number of N energy bands, with a bin size of Δt s, between the energy range of $[E_1, E_2]$. Here N , Δt , E_1 , E_2 are initially set as free parameters and determined by a series of trials on a burst-by-burst basis so that each of the light curves must have a signal-to-noise ratio $\sigma \geq 5$. The final choices of those parameters are listed in Table 1.
2. Lag calculation. We calculate spectral lags for any pair of light curves between the lowest energy band and any other band, using the method described in Zhang et al. (2012). As shown in Figure 1, we plot the lags for each burst as a function of E , the median of the energy boundaries of the higher energy bands. One can see that each of our sample exhibits a positive-to-negative lag transition.

3. THE MODEL

To model the observed lag- E behaviors in Figure 1, one has to consider the following two components:

1. The intrinsic lag, Δt_{int} , due to the GRB radiation itself. As pointed out in §1, the exact physical process causing spectral lags remains an open question. Nevertheless, some previous studies (e.g., Wei et al. 2017) assume a simple power law model for Δt_{int} . However, such a power law model doesn't account for the negative lags. In this study, we use a smoothly broken power-law function to model the energy-dependent lags, i.e., Δt_{int} is in form of

$$\Delta t_{\text{int}} = \zeta \left(\frac{E - E_0}{E_b} \right)^{\alpha_1} \left\{ \frac{1}{2} \left[1 + \left(\frac{E - E_0}{E_b} \right)^{1/\mu} \right] \right\}^{(\alpha_2 - \alpha_1)\mu}, \quad (1)$$

where ζ is the normalization amplitude, α_1 and α_2 are the two slopes before and after the transition energy, E_b and μ measures the smoothness of the transition. We note that when $\alpha_1 = \alpha_2$, Eq. (1) becomes a simple power law, as used in Wei et al. (2017).

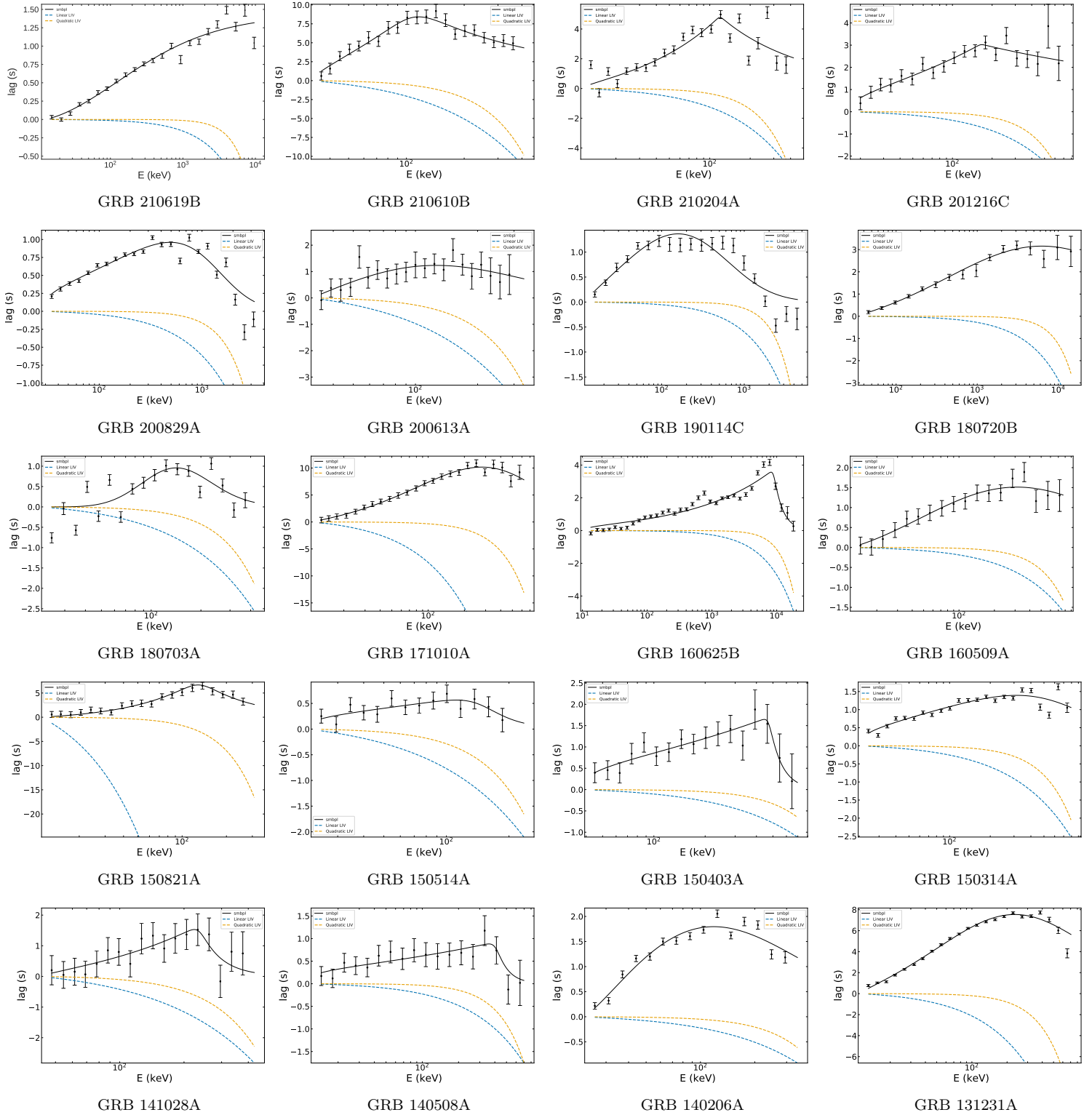


Figure 1. Lag-energy dependence of each GRB in our sample. Solid black lines show the smoothly broken power law (SBPL) fits. Blue and orange dotted lines indicate the maximally allowed LIV-induced lags in linear and quadratic cases, which define the lower limits of the QE energy for each GRB.

Table 1. List of the 32 GRBs in our sample and the corresponding parameters used for light curve extraction and lag calculation

GRB	Binsize (s)	N (Number of bands)	Energy interval for analysis (keV)	Time interval for analysis (s)	Redshift
GRB 210619B	0.1	24	[10, 11000]	[-5.0, 13.0]	1.937 ⁽¹⁾
GRB 210610B	0.3	22	[30, 380]	[10.0, 130.0]	1.13 ⁽²⁾
GRB 210204A	0.1	24	[10, 400]	[150.0, 300.0]	0.876 ⁽³⁾
GRB 201216C	0.1	21	[15, 700]	[-5.0, 50.0]	1.10 ⁽⁴⁾
GRB 200829A	0.1	24	[25, 3500]	[10.0, 35.0]	1.25 ⁽⁵⁾
GRB 200613A	0.08	22	[30, 300]	[-2.0, 50.0]	1.22 ⁽⁶⁾
GRB 190114C	0.1	21	[10, 5000]	[-1.0, 14.0]	0.425 ⁽⁷⁾
GRB 180720B	0.2	17	[25, 17000]	[-5.0, 25.0]	0.654 ⁽⁸⁾
GRB 180703A	0.1	19	[20, 400]	[-6.0, 35.0]	0.6678 ⁽⁹⁾
GRB 171010A	0.2	25	[10, 620]	[-8.0, 120.0]	0.3285 ⁽¹⁰⁾
GRB 160625B	0.1	29	[10, 20000]	[180.0, 215.7]	1.41 ⁽¹¹⁾
GRB 160509A	0.1	19	[10, 800]	[-3.0, 43.0]	1.17 ⁽¹²⁾
GRB 150821A	0.6	21	[10, 280]	[-5.0, 140.0]	0.755 ⁽¹³⁾
GRB 150514A	0.07	15	[20, 200]	[-2.0, 13.0]	0.807 ⁽¹⁴⁾
GRB 150403A	0.08	18	[35, 700]	[0.0, 35.0]	2.06 ⁽¹⁵⁾
GRB 150314A	0.08	24	[20, 800]	[-3.0, 20.0]	1.758 ⁽¹⁶⁾
GRB 141028A	0.1	19	[40, 400]	[-3.0, 45.0]	2.33 ⁽¹⁷⁾
GRB 140508A	0.07	19	[10, 720]	[-3.0, 20.0]	1.027 ⁽¹⁸⁾
GRB 140206A	0.07	16	[20, 320]	[-1.0, 20.0]	2.73 ⁽¹⁹⁾
GRB 131231A	0.1	24	[10, 713]	[-3.0, 63.0]	0.642 ⁽²⁰⁾
GRB 131108A	0.1	18	[20, 500]	[-3.0, 15.0]	2.40 ⁽²¹⁾
GRB 130925A	0.5	18	[10, 300]	[-10.0, 300.0]	0.347 ⁽²²⁾
GRB 130518A	0.1	17	[10, 1200]	[15.0, 42.0]	2.488 ⁽²³⁾
GRB 130427A	0.06	29	[10, 5000]	[2.0, 21.0]	0.3399 ⁽²⁴⁾
GRB 120119A	0.1	15	[25, 500]	[-5.0, 55.0]	1.728 ⁽²⁵⁾
GRB 100728A	0.3	18	[40, 400]	[0.0, 225.0]	1.567 ⁽²⁶⁾
GRB 091003A	0.1	17	[10, 800]	[12.0, 25.0]	0.8969 ⁽²⁷⁾
GRB 090926A	0.1	22	[10, 800]	[-2.0, 23.0]	2.1062 ⁽²⁸⁾
GRB 090618	0.1	21	[10, 700]	[40.0, 120.0]	0.54 ⁽²⁹⁾
GRB 090328	0.1	19	[30, 500]	[-8.0, 50.0]	0.736 ⁽³⁰⁾
GRB 081221	0.1	18	[10, 300]	[10.0, 43.0]	2.26 ⁽³¹⁾
GRB 080916C	0.1	19	[10, 600]	[-3.0, 55.0]	4.35 ⁽³²⁾

References—(1) GCN Circular 30272 (de Ugarte Postigo et al. 2021b), (2) GCN Circular 30194 (de Ugarte Postigo et al. 2021a), (3) GCN Circular 29432 (Xu et al. 2021), (4) GCN Circular 29077 (Vielfaure et al. 2020), (5) GCN Circular 28338(Oates et al. 2020), (6) GCN Circular 29320(de Ugarte Postigo 2020), (7) GCN Circular 23708(Castro-Tirado et al. 2019), (8) GCN Circular 22996(Vreeswijk et al. 2018), (9) GCN Circular 23889(Izzo et al. 2019), (10) GCN Circular 22096(de Ugarte Postigo et al. 2017), (11) GCN Circular 19600(Xu et al. 2016), (12) GCN Circular 18187(Tanvir et al. 2016), (13) GCN Circular 18187 (D’Elia et al. 2015), (14) GCN Circular 17822 (de Ugarte Postigo et al. 2015a), (15) GCN Circular 17672 (Pugliese et al. 2015), (16) GCN Circular 17583 (de Ugarte Postigo et al. 2015b), (17) GCN Circular 16983 (Xu et al. 2014a), (18) GCN Circular 16231 (Wiersema et al. 2014), (19) GCN Circular 15800 (Malesani et al. 2014), (20) GCN Circular 15645 (Xu et al. 2014b), (21) GCN Circular 15470(de Ugarte Postigo et al. 2013), (22) GCN Circular 15249(Vreeswijk et al. 2013), (23) GCN Circular 14685(Sanchez-Ramirez et al. 2013), (24) GCN Circular 14491 (Flores et al. 2013), (25) GCN Circular 12867(Milisavljevic et al. 2012), (26) GCN Circular 14500(Kruehler et al. 2013), (27) GCN Circular 10031(Cucchiara et al. 2009), (28) GCN Circular 9942(Malesani et al. 2009), (29) GCN Circular 9518 (Cenko et al. 2009), (30) GCN Circular 8766(de Ugarte Postigo et al. 2009), (31) Salvaterra et al. (2012), (32) Atwood et al. (2013)

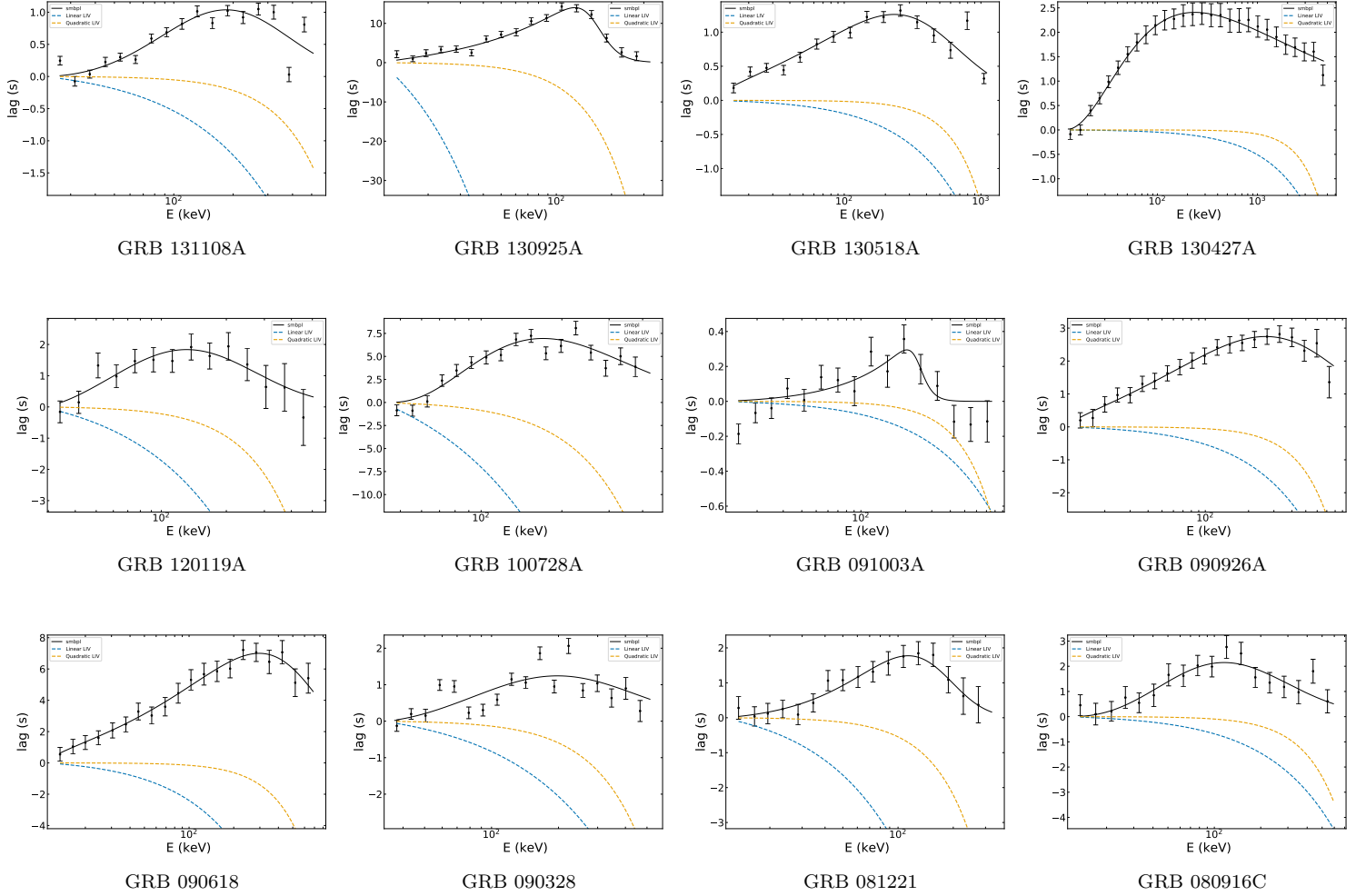


Figure 1.—Continued.

Table 2. Allowed range of the fitting parameters

Parameters	Range
ζ	[0.0, 4.0]
E_b	[0.0, 5000.0]
α_1	[-3.0, 10.0]
μ (G)	[0.0, 3.0]
α_2 (s)	[-10, 3]
$E_{QG,1}$ (GeV)	[0, 10^{20}]
$E_{QG,2}$ (GeV)	[0, 10^{15}]

2. The LIV lag. In the QG theory, a small-scale structure in spacetime can cause a deformed photon dispersion relation, which can be formulated as an (Amelino-Camelia et al. 1998; Jacob & Piran 2008):

$$c^2 p^2 = E^2 [1 + f(E/E_{QG})], \quad (2)$$

where c is the speed of light, p is the photon momentum, E_{QG} is the QG energy scale, $f(E/E_{QG})$ is the model-dependent function of the dimensionless ratio of E/E_{QG} . Noticing $f=0$ at $E=0$, f can be expanded as Taylor

series in a small energy condition ($E \ll E_{\text{QG}}$) at $a = 0$ as :

$$f = \sum_{n=0}^{\infty} \frac{f^{(n)}(a)}{n!} \left(\frac{E}{E_{\text{QG}}} - a \right)^n = \sum_{n=1}^{\infty} \frac{f^{(n)}(0)}{n!} \left(\frac{E}{E_{\text{QG}}} \right)^n. \quad (3)$$

Defining $E_{\text{QG},n}$ as the n th-order quantum gravity energy by

$$E_{\text{QG},n}^n = s_{\pm} E_{\text{QG}}^n \frac{n!}{f^{(n)}(0)}, \quad (4)$$

we can further substitute Eqs. (3) and (4) into Eq. (2), so

$$c^2 p^2 \simeq E^2 \left[1 + \sum_{n=1}^{\infty} s_{\pm} \left(\frac{E}{E_{\text{QG},n}} \right)^n \right], \quad (5)$$

where s_{\pm} represents the sign of the LIV effect. $s_{\pm} = +1$ (-1) corresponds to the subluminal (superluminal) scenario so the high energy photons travel slower (faster) than low energy photons. We only consider the case where $s_{\pm} = +1$ in this work to account for the negative lags.

In practice, it is convenient to replace the right side of Eq. (5) with its leading term in order n , so

$$c^2 p^2 \simeq E^2 \left[1 + s_{\pm} \left(\frac{E}{E_{\text{QG},n}} \right)^n \right]. \quad (6)$$

One can further derive the photon propagating speed as

$$v(E) = \frac{\partial E}{\partial p} \simeq c \left[1 - s_{\pm} \frac{n+1}{2} \left(\frac{E}{E_{\text{QG},n}} \right)^n \right]. \quad (7)$$

Eq. (7) suggests that two photons with different energy arrive at observers with a time delay, even both are emitted from one GRB concurrently. Considering cosmological expansion, the LIV-induced lag can be written as

$$\Delta t_{\text{LIV}} = -\frac{1+n}{2H_0} \frac{E^n - E_0^n}{E_{\text{QG},n}^n} \int_0^z \frac{(1+z')^n dz'}{\sqrt{\Omega_m (1+z')^3 + \Omega_\Lambda}}, \quad (8)$$

where the following cosmological parameters are adopted (Planck Collaboration et al. 2020): $H_0 = 67.36 \text{ km}\cdot\text{s}^{-1}\cdot\text{Mpc}^{-1}$, $\Omega_{m,0} = 0.315$, and $\Omega_{\Lambda,0} = 1 - \Omega_{m,0}$.

In this *Letter*, we consider both the linear ($n=1$) and quadratic ($n=2$) cases of Eq. (8), which, when fitted the observational data, can provide constraints on the corresponding QG energy scales, $E_{\text{QG},1}$ and $E_{\text{QG},2}$.

Finally, the observed energy-dependent lags can be modeled by

$$\tau = \Delta t_{\text{int}} + \Delta t_{\text{LIV}}, \quad (9)$$

which is directly fitted to the observational data in §4.

Table 3. Lower limits of Linear and Quadratic of Quantum Gravity Energy and the Best-fit Parameters of the SBPL Fit

GRB Name	Lower limits of $\log E_{\text{QG}}$ (GeV)		Best-fit Parameters of SBPL Model		
	Linear LIV	Quadratic LIV	α_1	α_2	E_{break} (keV)
GRB 210619B	$\geq 5.52 \times 10^{15}$	$\geq 1.72 \times 10^7$	$1.35^{+0.17}_{-0.46}$	$-0.85^{+0.33}_{-0.35}$	$46.13^{+29.83}_{-20.68}$
GRB 210610B	$\geq 3.23 \times 10^{13}$	$\geq 2.03 \times 10^5$	$0.68^{+0.49}_{-0.2}$	$-0.51^{+0.28}_{-0.57}$	$80.1^{+39.81}_{-10.17}$
GRB 210204A	$\geq 1.02 \times 10^{13}$	$\geq 1.31 \times 10^5$	$0.71^{+0.45}_{-0.36}$	$-0.64^{+0.62}_{-0.76}$	$107.89^{+66.86}_{-21.52}$
GRB 201216C	$\geq 1.9 \times 10^{14}$	$\geq 3.38 \times 10^5$	$0.42^{+0.21}_{-0.15}$	$-0.19^{+0.19}_{-0.22}$	$147.81^{+37.68}_{-39.02}$
GRB 200829A	$\geq 4.28 \times 10^{14}$	$\geq 2.52 \times 10^6$	$0.38^{+0.09}_{-0.05}$	$-3.53^{+1.0}_{-0.68}$	$1887.23^{+75.43}_{-57.0}$
GRB 200613A	$\geq 4.74 \times 10^{13}$	$\geq 1.68 \times 10^5$	$1.03^{+0.51}_{-0.48}$	$-3.38^{+2.08}_{-1.03}$	$381.27^{+9.85}_{-23.26}$
GRB 190114C	$\geq 5.43 \times 10^{14}$	$\geq 2.22 \times 10^6$	$0.94^{+0.72}_{-0.11}$	$-3.85^{+0.22}_{-0.36}$	$1754.88^{+14.11}_{-120.86}$
GRB 180720B	$\geq 9.54 \times 10^{14}$	$\geq 6.46 \times 10^6$	$3.21^{+0.56}_{-0.71}$	$-2.57^{+0.63}_{-0.63}$	$839.9^{+169.8}_{-39.86}$
GRB 180703A	$\geq 3.6 \times 10^{13}$	$\geq 1.19 \times 10^5$	$3.64^{+2.45}_{-1.38}$	$-5.21^{+0.81}_{-0.29}$	$155.11^{+47.98}_{-65.16}$
GRB 171010A	$\geq 5.68 \times 10^{13}$	$\geq 9.96 \times 10^4$	$0.9^{+0.03}_{-0.15}$	$-4.15^{+0.76}_{-1.0}$	$1473.3^{+26.52}_{-69.51}$
GRB 160625B	$\geq 1.35 \times 10^{15}$	$\geq 7.28 \times 10^6$	$0.36^{+0.04}_{-0.02}$	$-3.21^{+1.14}_{-1.94}$	$8862.15^{+800.83}_{-668.15}$
GRB 160509A	$\geq 1.73 \times 10^{14}$	$\geq 5.21 \times 10^5$	$1.64^{+0.12}_{-0.61}$	$-1.75^{+0.54}_{-0.24}$	$354.19^{+32.02}_{-36.81}$
GRB 150821A	$\geq 1.01 \times 10^{13}$	$\geq 1.1 \times 10^5$	$1.0^{+0.34}_{-0.11}$	$-1.19^{+0.82}_{-0.82}$	$119.55^{+42.72}_{-2.56}$
GRB 150514A	$\geq 3.57 \times 10^{13}$	$\geq 1.3 \times 10^5$	$0.34^{+0.19}_{-0.12}$	$-3.38^{+1.07}_{-0.27}$	$128.37^{+20.68}_{-27.98}$
GRB 150403A	$\geq 2.18 \times 10^{14}$	$\geq 5.8 \times 10^5$	$0.35^{+0.14}_{-0.06}$	$-5.55^{+1.29}_{-0.45}$	$433.61^{+27.42}_{-51.16}$
GRB 150314A	$\geq 3.91 \times 10^{14}$	$\geq 8.5 \times 10^5$	$0.38^{+0.13}_{-0.06}$	$-1.9^{+0.62}_{-0.52}$	$913.34^{+33.66}_{-13.27}$
GRB 141028A	$\geq 1.53 \times 10^{14}$	$\geq 2.75 \times 10^5$	$0.77^{+0.26}_{-0.22}$	$-3.72^{+0.19}_{-0.36}$	$192.74^{+29.62}_{-16.13}$
GRB 140508A	$\geq 1.21 \times 10^{14}$	$\geq 4.77 \times 10^5$	$0.27^{+0.57}_{-0.24}$	$-4.58^{+1.0}_{-0.42}$	$393.97^{+133.49}_{-125.62}$
GRB 140206A	$\geq 4.57 \times 10^{14}$	$\geq 9.33 \times 10^5$	$1.63^{+2.36}_{-0.68}$	$-2.15^{+1.21}_{-2.35}$	$152.58^{+22.67}_{-84.54}$
GRB 131231A	$\geq 2.09 \times 10^{13}$	$\geq 1.91 \times 10^5$	$0.81^{+0.1}_{-0.09}$	$-1.14^{+0.5}_{-0.13}$	$318.34^{+42.66}_{-140.88}$
GRB 131108A	$\geq 2.1 \times 10^{14}$	$\geq 6.04 \times 10^5$	$1.75^{+1.05}_{-0.56}$	$-6.9^{+0.1}_{-0.41}$	$612.89^{+63.75}_{-227.96}$
GRB 130925A	$\geq 8.18 \times 10^{12}$	$\geq 6.15 \times 10^4$	$0.84^{+0.14}_{-0.11}$	$-6.49^{+1.1}_{-1.62}$	$152.94^{+4.67}_{-10.65}$
GRB 130518A	$\geq 2.55 \times 10^{14}$	$\geq 1.64 \times 10^6$	$0.55^{+0.24}_{-0.16}$	$-2.32^{+1.25}_{-1.02}$	$591.49^{+160.03}_{-307.74}$
GRB 130427A	$\geq 3.85 \times 10^{14}$	$\geq 2.75 \times 10^6$	$3.94^{+0.02}_{-0.63}$	$-0.3^{+0.09}_{-0.1}$	$7.34^{+10.01}_{-2.0}$
GRB 120119A	$\geq 1.25 \times 10^{14}$	$\geq 2.97 \times 10^5$	$1.47^{+0.51}_{-0.55}$	$-6.17^{+2.23}_{-1.12}$	$447.46^{+32.16}_{-34.64}$
GRB 100728A	$\geq 3.46 \times 10^{13}$	$\geq 2.15 \times 10^5$	$7.98^{+1.98}_{-2.17}$	$-12.79^{+4.22}_{-0.58}$	$799.79^{+95.55}_{-198.37}$
GRB 091003A	$\geq 2.34 \times 10^{14}$	$\geq 6.22 \times 10^5$	$1.1^{+2.41}_{-1.1}$	$-8.27^{+5.28}_{-4.95}$	$231.06^{+62.0}_{-120.62}$
GRB 090926A	$\geq 1.09 \times 10^{14}$	$\geq 8.45 \times 10^5$	$0.64^{+0.1}_{-0.11}$	$-2.66^{+0.6}_{-1.09}$	$1048.68^{+97.2}_{-102.28}$
GRB 090618	$\geq 4.01 \times 10^{13}$	$\geq 1.97 \times 10^5$	$0.59^{+0.07}_{-0.07}$	$-4.14^{+0.14}_{-0.88}$	$947.71^{+37.42}_{-30.69}$
GRB 090328	$\geq 6.17 \times 10^{13}$	$\geq 2.17 \times 10^5$	$1.49^{+0.8}_{-0.8}$	$-5.14^{+1.45}_{-1.76}$	$620.23^{+66.86}_{-20.2}$
GRB 081221	$\geq 7.14 \times 10^{13}$	$\geq 2.41 \times 10^5$	$1.2^{+0.89}_{-0.71}$	$-8.7^{+1.85}_{-1.25}$	$252.52^{+69.84}_{-83.12}$
GRB 080916C	$\geq 6.45 \times 10^{14}$	$\geq 1.22 \times 10^6$	$3.34^{+0.66}_{-0.81}$	$-5.81^{+1.29}_{-1.17}$	$368.55^{+145.0}_{-100.22}$

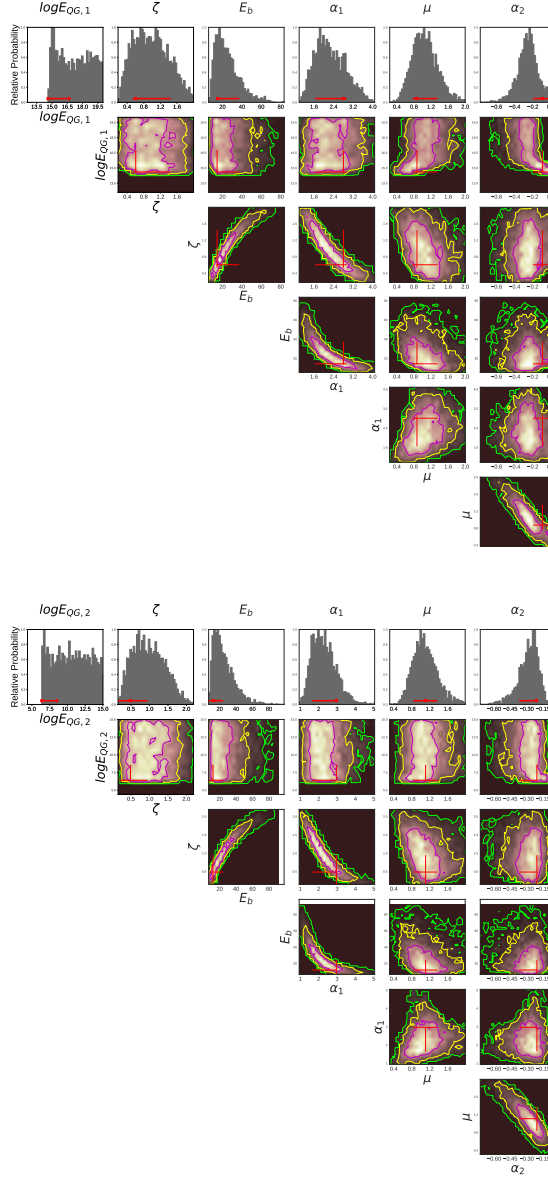


Figure 2. Distribution of posterior probability of parameters of linear and quadratic model for GRB 130427A. Upper panel: Gray histograms and contours represents the distributions of posterior probability of parameters for linear LIV model in one and two dimensions. Red arrows for parameter E_{QG} indicates its lower limits and red crosses show the best-fit values and their $1-\sigma$ error ranges. Lower panel: same but for quadratic ($n = 2$) case.

4. THE FIT

For each burst, we first fit its observed lags using the smoothly broken power-law as shown in Eq. (1). We can use this information to determine various features of the lag behavior, such as the break energy E_b , and the slopes prior and post E_b . The fit is performed using the *McEasyFit* (Zhang et al. 2015) tool, which is a self-developed Bayesian Monte-Carlo fitting package ensuring reliable and realistic best-fit parameters and their uncertainties based on converged Markov chains. The priors of the free parameters are set to uniform distributions in the range listed in

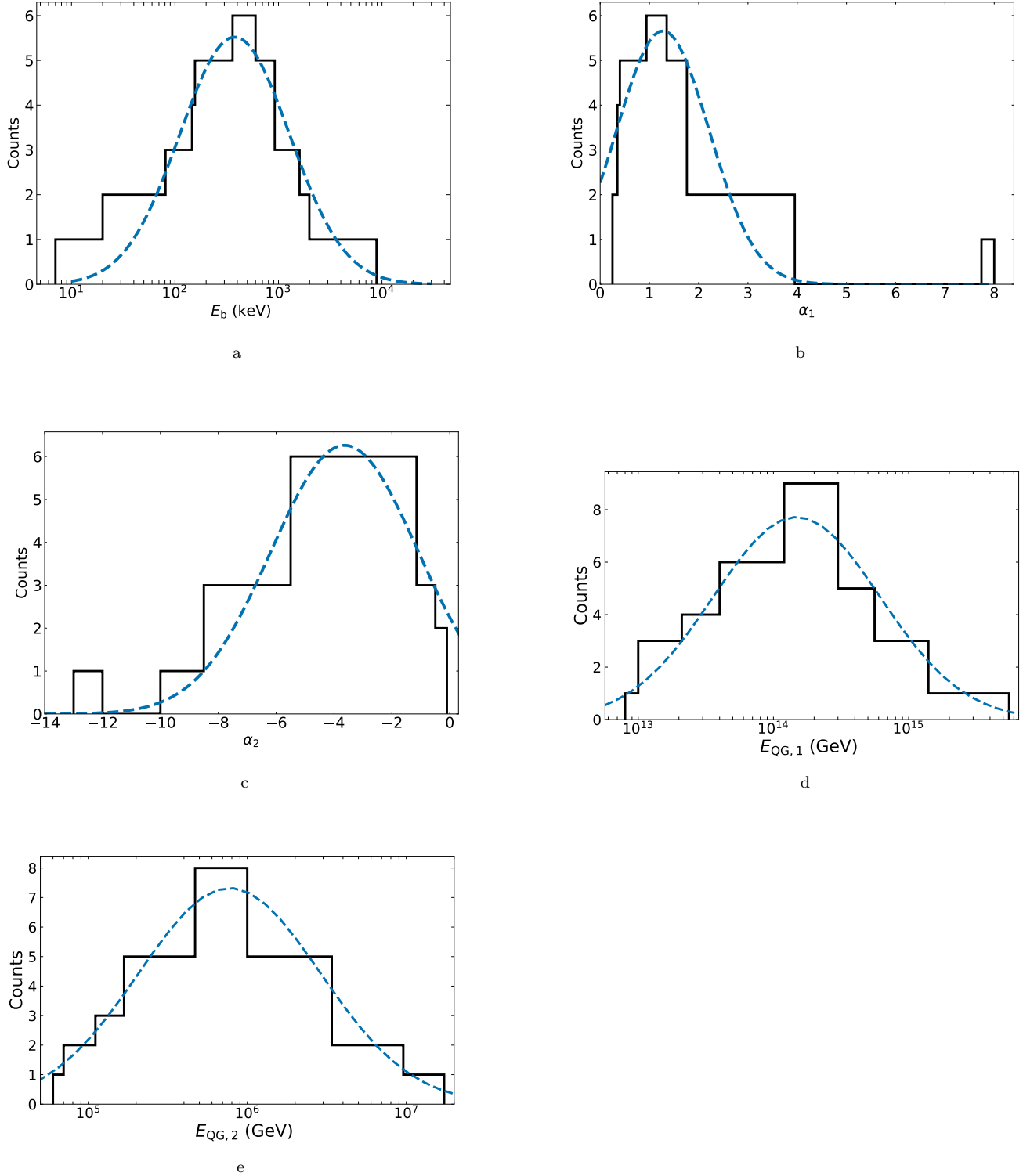


Figure 3. The distributions of the best-fit parameters (E_b, α_1, α_2) of the SBPL model and the constrained lower limits of the quantum gravity energy ($E_{QG,1}, E_{QG,2}$). Each distribution is fitted by a Gaussian or log-normal function.

Table 2. Our model successfully fit the data. The best-fit parameters as well as their constraints are listed in Table 3. The model-predicted curves using the best-fit parameters are over-plotted as black solid lines in each panel of Figure 1.

Next, we fit the observed data with the LIV-induced model as in Eq. (9). This introduces an additional free parameter, $E_{\text{QG},n}$. The prior of $E_{\text{QG},n}$ is set as a uniform distribution in logarithmic scale in range of $[0, 10^{20}]$ GeV for $n=1$, or $[0, 10^{15}]$ GeV for $n=2$ (Table 2). In addition, we require the Δt_{LIV} term in Eq. (9) not to dominate over Δt_{int} so that Δt_{int} still shows a negative-to-positive transition in order to be consistent with the observations. Such a requirement can be reflected in the log-likelihood function in *McEasyFit* as:

$$L(\Theta) = \begin{cases} -\infty & \alpha_1 < \alpha_2 \\ -\frac{1}{2}\Sigma \left(\frac{\tau_{\text{obs}} - \tau_{\text{model}}(\Theta)}{\sigma(\tau_{\text{obs}})} \right)^2 & \alpha_1 \geq \alpha_2 \end{cases}, \quad (10)$$

where Θ represents the free fitting parameters. The above approach allowed us to successfully fit the observed data of each GRB and constrain the lower limits of its linear and quadratic quantum gravity energies. Figure 2 shows an example of the posterior probability distributions of fitting parameters for GRB 130427A. For all of the GRBs in our sample, the E_{QG} lower limits are listed in Table 3 and correspond to the dashed lines in Figure 1.

Upon fitting the entire sample of 32 GRBs, we obtained the following key statistical properties of the lag behavior, as well as the constraints on the quantum gravity energy:

1. The distribution of the lag transition energy, E_b is a log-normal shape with a median value of $E_b = 398$ keV (Figure 3a);
2. The slopes for the $\tau - E$ relation prior and post the break are distributed as a Gaussian function. The median values of the α_1 and α_2 are 1.27 and -3.52 respectively (Figure 3b and Figure 3c);
3. The linear quantum gravity energy lower limits are constrained at a large range from 8.2×10^{12} GeV to 5.5×10^{15} GeV. The distribution of the lower limits is a log-normal shape with a median value of 1.5×10^{14} GeV (Figure 3d);
4. The quadratic quantum gravity energy lower limits are also constrained at a large range from 6.2×10^4 GeV to 1.7×10^7 GeV. The distribution of the lower limits is a log-normal shape with a median value of 8×10^5 GeV (Figure 3e).

5. SUMMARY & DISCUSSIONS

In this study, a total of 32 GRBs with positive-to-negative transitions in their spectral lags have been found among the 135 *Fermi*/GBM long GRBs with redshift measurement, suggesting lag transitions are not uncommon. We systematically processed and analyzed the lags of these 32 GRBs. The observed lag-E relationship of each burst can successfully be fitted by an empirically smoothly broken power-law function. Such fits yield a typical value of 400 keV for the transition energy. Our results are further applied to constrain the Lorentz invariance violation. Incorporating the LIV effect into the fit, the lower limits of linear and quadratic quantum gravity energy are derived for each burst. The typical lower limits of $E_{\text{QG},1} \geq 1.5 \times 10^{14}$ GeV and $E_{\text{QG},2} \geq 8 \times 10^5$ GeV of our study are consistent with, and sometimes deeper than, those of previous case studies, such as for GRB 160625B (Wei et al. 2017) and GRB 190114C (Du et al. 2021).

Our findings offer some insight into understanding the lag origins. For instance, some significant negative lags (e.g., $\tau \simeq 1$ s is observed in several GRBs) cannot be explained solely by the LIV effect. Thus the SBPL function we proposed in this work appears to be more accurate than the simple power law function (Wei et al. 2017) to describe the intrinsic lag behaviors in our sample. In addition, our study provides a rich sample for investigating the underlying physical processes that result in the lag transition. These theories include, but are not limited to, the hard-to-soft evolution of a curved spectrum (Liang & Kargatis 1996; Lu et al. 2012) and modified photosphere models (Meng et al. 2018, 2019, 2022).

ACKNOWLEDGEMENTS

Z.-K.L. thanks Ken Chen for the helpful discussion on this paper. We acknowledges support by the National Key Research and Development Programs of China (2018YFA0404204), the National Natural Science Foundation of China (Grant Nos. 11833003, U2038105, 12121003), the science research grants from the China Manned Space Project with NO.CMS-CSST-2021-B11, and the Program for Innovative Talents, Entrepreneur in Jiangsu. Y.-Z.M. is supported by the National Postdoctoral Program for Innovative Talents (grant no. BX20200164). We acknowledge the use of public data from the Fermi Science Support Center (FSSC).

REFERENCES

- Abdo, A. A., Ackermann, M., Ajello, M., et al. 2009a, *Nature*, 462, 331, doi: [10.1038/nature08574](https://doi.org/10.1038/nature08574)
- Abdo, A. A., Ackermann, M., Arimoto, M., et al. 2009b, *Science*, 323, 1688, doi: [10.1126/science.1169101](https://doi.org/10.1126/science.1169101)
- Acciari, V. A., Ansoldi, S., Antonelli, L. A., et al. 2020, *PhRvL*, 125, 021301, doi: [10.1103/PhysRevLett.125.021301](https://doi.org/10.1103/PhysRevLett.125.021301)
- Amelino-Camelia, G. 2013, *Living Reviews in Relativity*, 16, 5, doi: [10.12942/lrr-2013-5](https://doi.org/10.12942/lrr-2013-5)
- Amelino-Camelia, G., Ellis, J., Mavromatos, N. E., Nanopoulos, D. V., & Sarkar, S. 1998, *Nature*, 393, 763, doi: [10.1038/31647](https://doi.org/10.1038/31647)
- Atwood, W. B., Baldini, L., Bregeon, J., et al. 2013, *ApJ*, 774, 76, doi: [10.1088/0004-637X/774/1/76](https://doi.org/10.1088/0004-637X/774/1/76)
- Castro-Tirado, A. J., Hu, Y., Fernandez-Garcia, E., et al. 2019, GRB Coordinates Network, 23708, 1
- Cenko, S. B., Perley, D. A., Junkkarinen, V., et al. 2009, GRB Coordinates Network, 9518, 1
- Cucchiara, A., Fox, D. B., Cenko, S. B., Tanvir, N., & Berger, E. 2009, GRB Coordinates Network, 1031, 1
- de Ugarte Postigo, A. 2020, GRB Coordinates Network, 29320, 1
- de Ugarte Postigo, A., Jakobsson, P., Malesani, D., et al. 2009, GRB Coordinates Network, 8766, 1
- de Ugarte Postigo, A., Selsing, J., Malesani, D., et al. 2017, GRB Coordinates Network, 22096, 1
- de Ugarte Postigo, A., Thoene, C., Agui Fernandez, J. F., et al. 2021a, GRB Coordinates Network, 30194, 1
- . 2021b, GRB Coordinates Network, 30272, 1
- de Ugarte Postigo, A., Thoene, C. C., Gorosabel, J., et al. 2013, GRB Coordinates Network, 15470, 1
- de Ugarte Postigo, A., Xu, D., Malesani, D., & Tanvir, N. R. 2015a, GRB Coordinates Network, 17822, 1
- de Ugarte Postigo, A., Fynbo, J. P. U., Thoene, C., et al. 2015b, GRB Coordinates Network, 17583, 1
- D'Elia, V., Kruehler, T., Wiersema, K., et al. 2015, GRB Coordinates Network, 18187, 1
- Du, S.-S., Lan, L., Wei, J.-J., et al. 2021, *ApJ*, 906, 8, doi: [10.3847/1538-4357/abc624](https://doi.org/10.3847/1538-4357/abc624)
- Flores, H., Covino, S., Xu, D., et al. 2013, GRB Coordinates Network, 14491, 1
- Ioka, K., & Nakamura, T. 2001, *ApJL*, 554, L163, doi: [10.1086/321717](https://doi.org/10.1086/321717)
- Izzo, L., de Ugarte Postigo, A., Schady, P., et al. 2019, GRB Coordinates Network, 23889, 1
- Jacob, U., & Piran, T. 2008, *JCAP*, 2008, 031, doi: [10.1088/1475-7516/2008/01/031](https://doi.org/10.1088/1475-7516/2008/01/031)
- Kruehler, T., Greiner, J., & Kann, D. A. 2013, GRB Coordinates Network, 14500, 1
- Li, Z. 2010, *ApJ*, 709, 525, doi: [10.1088/0004-637X/709/1/525](https://doi.org/10.1088/0004-637X/709/1/525)
- Liang, E., & Kargatis, V. 1996, *Nature*, 381, 49, doi: [10.1038/381049a0](https://doi.org/10.1038/381049a0)
- Lu, R.-J., Wei, J.-J., Liang, E.-W., et al. 2012, *ApJ*, 756, 112, doi: [10.1088/0004-637X/756/2/112](https://doi.org/10.1088/0004-637X/756/2/112)
- Malesani, D., Goldoni, P., Fynbo, J. P. U., et al. 2009, GRB Coordinates Network, 9942, 1
- Malesani, D., Xu, D., Fynbo, J. P. U., et al. 2014, GRB Coordinates Network, 15800, 1
- Mattingly, D. 2005, *Living Reviews in Relativity*, 8, 5, doi: [10.12942/lrr-2005-5](https://doi.org/10.12942/lrr-2005-5)
- Meng, Y.-Z., Geng, J.-J., & Wu, X.-F. 2022, *MNRAS*, 509, 6047, doi: [10.1093/mnras/stab3132](https://doi.org/10.1093/mnras/stab3132)
- Meng, Y.-Z., Liu, L.-D., Wei, J.-J., Wu, X.-F., & Zhang, B.-B. 2019, *ApJ*, 882, 26, doi: [10.3847/1538-4357/ab30c7](https://doi.org/10.3847/1538-4357/ab30c7)
- Meng, Y.-Z., Geng, J.-J., Zhang, B.-B., et al. 2018, *ApJ*, 860, 72, doi: [10.3847/1538-4357/aac2d9](https://doi.org/10.3847/1538-4357/aac2d9)
- Milisavljevic, D., Drout, M., & Berger, E. 2012, GRB Coordinates Network, 12867, 1
- Norris, J. P., & Bonnell, J. T. 2006, *ApJ*, 643, 266, doi: [10.1086/502796](https://doi.org/10.1086/502796)
- Norris, J. P., Marani, G. F., & Bonnell, J. T. 2000, *ApJ*, 534, 248, doi: [10.1086/308725](https://doi.org/10.1086/308725)
- Norris, J. P., Nemiroff, R. J., Bonnell, J. T., et al. 1996, *ApJ*, 459, 393, doi: [10.1086/176902](https://doi.org/10.1086/176902)
- Oates, S. R., Kuin, N. P. M., De Pasquale, M., et al. 2020, GRB Coordinates Network, 28338, 1
- Planck Collaboration, Aghanim, N., Akrami, Y., et al. 2020, *A&A*, 641, A6, doi: [10.1051/0004-6361/201833910](https://doi.org/10.1051/0004-6361/201833910)
- Pugliese, V., Xu, D., Tanvir, N. R., et al. 2015, GRB Coordinates Network, 17672, 1

- Salmonson, J. D. 2000, ApJL, 544, L115,
doi: [10.1086/317305](https://doi.org/10.1086/317305)
- Salvaterra, R., Campana, S., Vergani, S. D., et al. 2012,
ApJ, 749, 68, doi: [10.1088/0004-637X/749/1/68](https://doi.org/10.1088/0004-637X/749/1/68)
- Sanchez-Ramirez, R., Gorosabel, J., Castro-Tirado, A. J.,
Cepa, J., & Gomez-Velarde, G. 2013, GRB Coordinates
Network, 14685, 1
- Schaefer, B. E. 2004, ApJ, 602, 306, doi: [10.1086/380898](https://doi.org/10.1086/380898)
- Shen, R.-F., Song, L.-M., & Li, Z. 2005, MNRAS, 362, 59,
doi: [10.1111/j.1365-2966.2005.09163.x](https://doi.org/10.1111/j.1365-2966.2005.09163.x)
- Tanvir, N. R., Levan, A. J., Cenko, S. B., et al. 2016, GRB
Coordinates Network, 19419, 1
- Toma, K., Wu, X.-F., & Mészáros, P. 2009, ApJ, 707, 1404,
doi: [10.1088/0004-637X/707/2/1404](https://doi.org/10.1088/0004-637X/707/2/1404)
- Uhm, Z. L., & Zhang, B. 2016, ApJ, 825, 97,
doi: [10.3847/0004-637X/825/2/97](https://doi.org/10.3847/0004-637X/825/2/97)
- Vielfaure, J. B., Izzo, L., Xu, D., et al. 2020, GRB
Coordinates Network, 29077, 1
- von Kienlin, A., Meegan, C. A., Paciesas, W. S., et al. 2020,
ApJ, 893, 46, doi: [10.3847/1538-4357/ab7a18](https://doi.org/10.3847/1538-4357/ab7a18)
- Vreeswijk, P. M., Malesani, D., Fynbo, J. P. U., De Cia, A.,
& Ledoux, C. 2013, GRB Coordinates Network, 15249, 1
- Vreeswijk, P. M., Kann, D. A., Heintz, K. E., et al. 2018,
GRB Coordinates Network, 22996, 1
- Wang, X. I., Zheng, X., Xiao, S., et al. 2021, ApJ, 922, 237,
doi: [10.3847/1538-4357/ac29bd](https://doi.org/10.3847/1538-4357/ac29bd)
- Wei, J.-J., Zhang, B.-B., Shao, L., Wu, X.-F., & Mészáros,
P. 2017, ApJL, 834, L13,
doi: [10.3847/2041-8213/834/2/L13](https://doi.org/10.3847/2041-8213/834/2/L13)
- Wiersema, K., Tanvir, N., Levan, A., & Karjalainen, R.
2014, GRB Coordinates Network, 16231, 1
- Xu, D., Levan, A. J., Fynbo, J. P. U., et al. 2014a, GRB
Coordinates Network, 16983, 1
- Xu, D., Malesani, D., Fynbo, J. P. U., et al. 2016, GRB
Coordinates Network, 19600, 1
- Xu, D., Malesani, D., Tanvir, N. R., et al. 2014b, GRB
Coordinates Network, 15645, 1
- Xu, D., Izzo, L., Fynbo, J. P. U., et al. 2021, GRB
Coordinates Network, 29432, 1
- Yang, J., Chand, V., Zhang, B.-B., et al. 2020, ApJ, 899,
106, doi: [10.3847/1538-4357/aba745](https://doi.org/10.3847/1538-4357/aba745)
- Yi, T., Liang, E., Qin, Y., & Lu, R. 2006, MNRAS, 367,
1751, doi: [10.1111/j.1365-2966.2006.10083.x](https://doi.org/10.1111/j.1365-2966.2006.10083.x)
- Zhang, B.-B., van Eerten, H., Burrows, D. N., et al. 2015,
ApJ, 806, 15, doi: [10.1088/0004-637X/806/1/15](https://doi.org/10.1088/0004-637X/806/1/15)
- Zhang, B.-B., Zhang, B., Liang, E.-W., et al. 2011, ApJ,
730, 141, doi: [10.1088/0004-637X/730/2/141](https://doi.org/10.1088/0004-637X/730/2/141)
- Zhang, B.-B., Burrows, D. N., Zhang, B., et al. 2012, ApJ,
748, 132, doi: [10.1088/0004-637X/748/2/132](https://doi.org/10.1088/0004-637X/748/2/132)
- Zhang, B. B., Liu, Z. K., Peng, Z. K., et al. 2021, Nature
Astronomy, 5, 911, doi: [10.1038/s41550-021-01395-z](https://doi.org/10.1038/s41550-021-01395-z)